Accepted: The Journal of Physical Chemistry C

Low-Temperature CO Oxidation over Combustion Made Fe- and Cr Doped Co_3O_4 Catalysts: Role of Dopant's Nature toward Achieving Superior Catalytic Activity and Stability

Tinku Baidya[a,*], Toru Murayama[b,*], Parthasarathi Bera[c,*], Olga V. Safonova[d], Patrick Steiger[d], Devide Ferri[d], Nirmal Kumar Katiyar[e], Krishanu Biswas[e], Masatake Haruta[b]

[a] Department of Mechanical and Aerospace Engineering, University of California, 9500 Gilman Drive, San Diego, CA 92093, United States of America

[b] Department of Applied Chemistry, Graduate School of Urban Environmental Sciences, Tokyo Metropolitan University, 1-1 Minami-osawa, Hachioji, Tokyo 192-0397, Japan

[c] Surface Engineering Division, CSIR–National Aerospace Laboratories, Bengaluru 560017, India

[d] Paul Scherrer Institut, 5253 Villigen, Switzerland

[e] Department of Materials Science and Engineering, Indian Institute of Technology Kanpur, Kanpur 208016, India

Abstract

Co_3O_4 with spinel structure shows unique activity for CO oxidation at low temperature under dry condition, which is very sensitive to the synthesis method. In this study, Fe and Cr doped Co_3O_4 catalysts were prepared by highly exothermic solution combustion technique and tested for low-temperature CO oxidation. The enhanced catalytic activities correlate to the redox behavior of dopants. While Fe/Co_3O_4 compositions demonstrate maximal activity for 15% Fe substitution with T_{50} at – 85 °C, which remains almost constant up to 25% of Fe, the incorporation of Cr^{3+} decreases the activity passing through a maximum for 7% of Cr with T_{50} at –42 °C. The substitution of Cr and Fe occurred in octahedral site of the Co_3O_4 lattice and both Cr and Fe majorly remain in +3 state. The exposed surfaces in Fe and Cr doped Co_3O_4 crystallites are mainly (111) and (220). 15% Fe/Co_3O_4 calcined at 500 and 600 °C still demonstrate high catalytic activity with 100% CO conversion below –60 °C indicating stability of exposed surfaces. H_2 TPR shows similar reducibility for all Fe doped Co_3O_4 catalysts, while addition of non-reducible Cr dopant shifts the reduction profiles toward higher temperatures indicating stronger Co^{3+}–O bond in Cr/Co_3O_4 samples. As the Fe^{3+}/Fe^{2+} redox couple partly substitutes the Co^{3+}/Co^{2+} couple, redox property of Co^{3+} species remains unperturbed which leads to higher

activity for low temperature CO oxidation in Fe/Co_3O_4. On the other hand, Cr^{3+} reduces the concentration of active Co^{3+} sites as well as stronger Cr-O bond in Cr/Co_3O_4 surface which results in the gradual decrease of CO conversion.

***Corresponding authors:**

1. Email: tinku26@gmail.com

Present address: Department of Mechanical and Aerospace Engineering, University of California, 9500 Gilman Drive, San Diego, CA 92093, United States of America

2. E-mail: murayama@tmu.ac.jp

Present address: Department of Applied Chemistry, Graduate School of Urban Environmental Sciences, Tokyo Metropolitan University, 1-1 Minami-osawa, Hachioji, Tokyo 192-0397, Japan

3. Email: partho@nal.res.in

Surface Engineering Division, CSIR–National Aerospace Laboratories, Bengaluru 560017, India

1. Introduction

Removal of CO, mainly by oxidation at ambient temperature is useful for in-door air quality control [1], purification of H_2 for fuel cells [2], pure N_2 and O_2 gas production from air in the semiconductor industry [3], gas sensing of CO traces [4] and so forth. The extensive studies of CO oxidation also results from the fact that this reaction is structure sensitive and rather simple for mechanistic model studies.

The pioneering work by Haruta and coworkers have demonstrated high activity for CO oxidation over supported gold nanoparticles [5–7]. However, gold-based catalysts are very costly, and thus, cheaper alternatives with similar activity would be highly desirable. Considerable efforts have been concentrated on the development of CO oxidation catalyst based on transition metal oxides and some basic oxides such as Co_3O_4, NiO etc., and a mixture of

MnO_2 and CuO (called Hopcalite) have been found active at room temperature for CO oxidation in presence of moisture [8–16]. Among transition metal oxides, Co_3O_4 has received the highest interest due to its low-temperature catalytic activity under dry conditions (below 10 ppm H_2O) [17–20]. Co_3O_4 prepared by different methods have shown different CO oxidation activities due to variation in to surface area related crystallite size, crystal surface morphology and surface structure etc [18, 21–26]. Xu and coworkers have prepared Co_3O_4 nanosheets by an in-situ de-alloying method combined with an oxidation process and the resulting catalyst demontrated a full CO conversion at around 110 °C [15]. Through a nanocasting process, Tüysüz et al. have synthesized mesoporous Co_3O_4 that have shown excellent CO oxidation activity at ambient temperature [16]. Teng and coworkers have demonstrated that the nature surface planes, which depend on crystal morphology of shaped Co_3O_4 nanocrystals, determine the activity for CO oxidation [23]. Interestingly, Co_3O_4 nanorods with predominantly exposed (110) surfaces have exhibited very high activity for CO oxidation at −77 °C under normal conditions [18]. Wang et al. have calculated energetics for CO activation on different faces of Co_3O_4 crystals and established the changes in the reactivity in the following order: (110) > (100) > (111) [25]. It has also been pointed out that Co^{3+} concentration in these planes correlates to the low temperature reactivity. This promotes the idea of preparation of active catalyst through morphology-controlled synthesis, which ensures exposure of specific active plains at the surface. In most cases, however, it is difficult to prepare solid catalysts that have such preferentially exposed active faces, and even if specific morphology is obtained, it may not be stable under reaction conditions, especially at high temperatures. Therefore, since preparation of pure Co_3O_4 requires ambient condition for retaining sensitive surface feature for high activity, doping of different metal ions has been interesting.

Several metals have been doped in Co_3O_4 to improve its catalytic activity, although stability remained an issue. Within this context, the choice of dopant metal is very important. For example, while Fe doping has been found to improve the CO oxidation activity [27,28], Zn and Al substitution have reduced it [29] because Al–O bond has strong covalent nature due to AlO_4 motif formation as well as Zn which enhances the basic property by making the surface passive due to the formation of carbonate species. The catalytic promotion by using In and Bi as dopants have been reported [30,31], but the stability even at moderately higher temperature is highly doubtful as found in our results with Bi doping (unpublished). This problem arises because of a phase separation of these non-transition metal oxides. It is known that Co^{3+} acting as active site in Co_3O_4 should switch its oxidation state between +3 and +2. Because of similar nature and possibility for switching between +2 and +3 states, we considered Fe as very promissing for Co_3O_4 doping. By Fe doping the concentration of redox sites in the catalyst is expected to remain similar. Cr dopant was chosed for different reasons. If active Co^{3+} is replaced in Co_3O_4 structure by a non-easily reducible cation like Cr^{3+} the catalytic activity of Co_3O_4 should change. Therefore by using of Cr dopant, additional information on the nature of active sites can be obtained. Moreover, Fe and Cr are known to form less stable carbonates, which can minimize the possibility of involvement of other factors in the activity.

All the Co_3O_4 based catalysts reported in the literature have been prepared by mild condition followed by calcination at low temperature, mostly at 350 ^oC. Therefore, it would be interesting to study the activity of materials prepared by a harsh synthesis route as it is for solution combustion method. Moreover, solution combustion method is known to give highly homogeneous solid solutions [32,33] unlike other methods such as impregnation and co-precipitation. In the present study two series of Co_3O_4 oxides doped with Fe and Cr have been

prepared by single step solution combustion method. A systematic study of CO oxidation activity as a function of dopant concentration and detailed structural and morphological characterization of the catalysts have been carried out. The catalytic activities have been correlated with the dopant nature related to its redox activity.

2. Experimental details

Fe doped Co_3O_4 compounds were prepared by a solution combustion method using cobalt nitrate, ferric nitrate as precursors of Co and Fe and citric acid as fuel. For the preparation of 10% Fe/Co_3O_4, 10 g of $Co(NO_3)_2.6H_2O$ (Acros Organics, 99%), 1.542 g of $Fe(NO_3)_3.9H_2O$ (Sigma-Aldrich, 99.5%) and 6.68 g of citric acid (Macron, 99%) were taken in the molar ratio of 0.9:0.1:0.883. The precursor compounds were dissolved in 30 mL of water in a 300 mL crystallizing dish resulting in a clear solution. The dish was then kept in a furnace preheated to 400 °C. The evaporation led to the dehydration and then the combustion with a flame started yielding the voluminous solid product within a few minutes. Then, the solid product was grinded to a fine powder and calcined in air at 400 ^oC for 3 h to remove the residual carbon species. *These catalysts were named as-prepared/uncalcined samples.* Following similar procedure various compositions with different concentration of Fe ranging from 3% to 25% were also prepared. For the preparation of Cr doped Co_3O_4, stoichiometric amount of $Co(NO_3)_2.6H_2O$, $Cr(NO_3)_2.6H_2O$ (Alfa Aesar, 98.5%) and citric acid were taken following similar techniques and the Cr concentrations were varied from 1% to 33%.

Nitrogen physisorption isotherms (adsorption–desorption branches) were measured on Quanta chrome Autosorb Automated Gas Sorption System (Quantachrome Instruments) at 77 K. The samples were outgassed for 1 h under vacuum at 400 ^oC before the measurements and the specific surface area (SSA) was determined using the Brunauer Emmett Teller (BET) method.

X-ray diffraction (XRD) patterns of the catalysts were obtained with an X-ray diffractometer (BRUKER D2 PHASER) equipped with a monochromator for CuK_α radiation at a voltage of 30 kV and a current of 100 mA. Fine powder samples were used for the XRD measurements and were scanned from $2\theta = 10$ to 70° at the rate of 0.02° s^{-1}. The observed diffraction patterns were identified using the International Centre for Diffraction Data (ICDD) database.

Temperature-programmed reduction (TPR) studies of the catalysts were performed with a Quantachrome Instrument (ChemBET-3000 TPR/TPD) to investigate their reduction behaviors. Typically, 25 mg of the sample was placed in a U-shaped quartz tube and ramped from 40 to 700 °C at a 10 °C min^{-1} rate in a gas mixture containing 3% H_2/N_2. The consumption of H_2 during the reduction was monitored by a thermal conductivity detector (TCD). Prior to a TPR test, the sample was pretreated in oxygen gas flow at 400 °C for 15 min and then cooled down to room temperature in N_2 flow.

CO_2 temperature programmed desorption (TPD) was conducted using a home built test set-up. Prior to the measurements, the samples were pelletized, crushed and sieved to the size fraction of 100–200 micron. Required amounts of sample were loaded into a tubular quartz reactor and sandwiched between two quartz wool plugs. A tubular furnace was used to provide heating. A K-type thermocouple centered inside the catalyst bed was used to record the temperature. Prior to CO_2 adsorption the catalyst was heated to 400 °C in N_2 and cooled down to room temperature (< 28°C). This pretreatment was followed by 30 min saturation in 10 vol% CO_2 at room temperature before rinsing any excess CO_2 during 60 min of inert gas stream. The desorption experiments were conducted by ramping the temperature to 400 °C (5 °C min^{-1}) and simultaneously recording CO_2 concentration using a transmission infrared spectrometer

(NICOLET ANTARIS IGS Analyzer, Thermo Scientific). Total flow rates were kept constant at 15000 mL h^{-1} g^{-1} for pretreatment as well as TPD.

For transmission electron microscopy (TEM), the material was dispersed in ethanol and few drops were deposited onto a perforated carbon foil supported on a copper grid. TEM investigations were performed on a CM30ST microscope (FEI; LaB6 cathode, operated at 300 kV, point resolution ~2 Å). The lattice fringe images have been analyzed using software Gatan Digital Micrograph v. 2.31.734.0, where the d-spacing carefully have been calculated after regenerating the image from selected region (marked red square) with help of FFT (Fast Fourier Transform) and selected spots encircled in inset corresponding image.

The XPS of Fe and Cr doped Co_3O_4 solid solutions were recorded using a Thermo Fisher Scientific Multilab spectrometer with non-monochromatic Al K_α radiation (1486.6 eV) as an X-ray source operated at 150 W (12.5 kV and 12 mA). As Fe LMM and Co LMM peaks overlap with Co2p and Fe2p core level peaks, XPS of Fe/Co_3O_4 catalysts were carried out with Mg K_α radiation. All the spectra were obtained with a pass energy of 40 eV and a step increase of 0.05 eV. The CasaXPS program was employed for curve-fitting of the Co2p and Fe2p core level spectra into several components with Gaussian–Lorentzian peaks after Shirley background subtraction. Peak positions, spin–orbit splitting, doublet intensity ratios, and full width at half maximum (FWHM) were fixed as given in the literature.

X-ray absorption spectra at Cr and Fe K-edges were measured at SuperXAS beamline at the Swiss Light Source (Paul Scherrer Institute, Villigen, Switzerland) using the Si(111) channel cut monochromator. The rejection of higher harmonics and focusing were achieved by a Si-coated collimating mirror at 2.8 mrad and a rhodium-coated toroidal mirror at 2.8 mrad,

respectively. The size of the X-ray beam on the sample was 1.5 mm by 0.5 mm in horizontal and vertical directions, respectively, with a total intensity of about 5×10^{11} ph/s. The optimal amount of each sample was mixed with cellulose and pressed into pellets. The X-ray absorption spectra were measured in transmission mode using ionization chambers as the detectors. Reference foils of Cr (K edge at 5989 eV) and Fe (K edge at 7112 eV) were measured simultaneously with the samples for precise energy calibration. The spectra were reduced following the standard procedures in the Demeter program package [34]. Extended X-ray absorption fine structure (EXAFS) spectra at Cr K-edge were fitted in R-space between 1 and 5 Å using k weighting of 3 in the range between 3–12 $Å^{-1}$. EXAFS spectra at Fe K-edge were fitted in R-space between 1 and 5 Å using k weighting of 3 in the range between 3–10 $Å^{-1}$. Amplitude reduction factor (S_0^2) was fitted using Fe and Cr refrence foils.

Catalytic activity was tested through CO oxidation reaction. The catalyst (0.15 g) was placed in a fixed bed reactor and 1 vol% CO in air was flowed (50 mL min^{-1}). H_2O concentration in the flow gas was monitored by a dew-point meter, and the concentrations were 15–50 ppm at T_{50} (temperature for 50% CO conversion) in all experiments. T_{50} or T_{100} indicate a temperature for 50% or 100% CO conversion to compare the catalytic activity of the samples.

3. Results and discussion

3.1 Catalytic activities

The catalytic CO conversion curves as a function of temperature for $CO + O_2 = CO_2$ reaction over Fe and Cr doped Co_3O_4 catalysts are shown in the Figure 1(a,b) taking pure Co_3O_4 as a reference. The results indicate a systematic change of activity with gradually increasing concentration of Fe and Cr in Co_3O_4. Pure Co_3O_4 demonstrates the poorest activity among all the

catalysts, which significantly increases by doping of Fe and Cr. By comparing the CO conversion in the equivalent compositions of both catalysts series at any temperature, it becomes evident that Fe doped Co_3O_4 is more active than its Cr doped analogs (see Fig. 1 a, b). The activities of Fe doped Co_3O_4 increase with an increase in Fe content up to 15% and then there is almost no change up to 33% Fe content, especially up to 90% CO conversion. The CO conversion starts below –100 ^oC reaching T_{100} at – 60 ^oC over 15% Fe/Co_3O_4. On the other hand, highest CO conversion activity is gradually achieved with 7% Cr doping and then systematically decreases up to 33%. As conversion below 90% changes gradually with Fe concentrations, T_{100} is not consistent for the same. Therefore, T_{50} vs dopant concentrations in all catalysts is plotted in the Figure 2. T_{50} is shifted from 0 ^oC in pure Co_3O_4 to –85 ^oC in 15% Fe/Co_3O_4 achieving the maximal activity and then the activity remains almost unchanged up to of 25% of Fe. At the same time, In the Cr doped samples, T_{50} reaches the lowest value of –42 ^oC with 7% substitution and then gradually increases to higher temperatures reaching –20 ^oC in 33% Cr/Co_3O_4. Previous report showed that 100% Co^{3+} substitution with Cr^{3+} led to much lower activity for CO oxidation in $CoCr_2O_4$ [35]. Thus, there is a strong difference in activity between Fe and Cr doped Co_3O_4 catalysts which needs to be understood through structure studies and analysis of surface properties.

Based on above-mentioned screening of the catalysts activity, $15\%Fe/Co_3O_4$ was chosen for more detailed structural studies. Figure 3 shows a comparison of catalytic activity of this samples to the same sample calcined in air at 500 and 600 ^oC. Interestingly, calcined samples show 100% CO conversion below –60 °C similar to fresh sample except for a slight shift in the low conversion side. This indicates that the structure of the active surface have undergone only minor changes in Fe doped Co_3O_4 after calcination up to 600 ^oC.

3.2 BET surface area

The BET surface area of the Cr doped Co_3O_4 samples increases with higher doping of Cr as presented in Table 1. Clearly, surface area gradually increases from 12.73 $m^2\ g^{-1}$ in pure Co_3O_4 to 42.79 $m^2\ g^{-1}$ in 10% Cr doping. Similarly, Fe doped Co_3O_4 shows systematic increase in surface area from XX m^2g^{-1} in 3%Fe/Co_3O_4 to YY m^2g^{-1} in 25%Fe/Co_3O_4.

3.3 XRD studies

XRD profiles of the Fe and Cr doped Co_3O_4 samples are shown in Figure 4 (a,b). For Fe doped Co_3O_4 up to 25% Fe substitution, the XRD profiles indicate formation of solid solution retaining parent spinel structure. There were no reflection peaks related to FeO_x species as a separate phase even of low intensity. A systematic shift in peak positions of spinel structure toward lower angles (marked by dotted line) is observed with gradually increasing concentration of Fe indicating substitution of smaller sized Fe in the Co_3O_4 lattice. The distribution of substituted Fe in Co_3O_4 lattice was homogeneous (also see Figure S1). The peak widths was broadened and the crystallite size calculated using Scherrer formula (Crystallite size (nm) = $0.9\lambda/\beta Cos\theta$) at several high intensity peaks are presented in Table 1. There is a systematic decrease in crystallite size changing from 33 nm in Co_3O_4 to 14 nm in 25% Fe/Co_3O_4. The XRD profiles of 15%Fe/Co_3O_4 having optimal Fe concentration were also measured after calculation at different temperatures and in Figure S2. The results indicate slight increase in peaks width after calcinations at 600 ^{0}C which can be explain by sintering.

XRD profiles of Cr doped Co_3O_4 samples are in the Figure 4b indicating incorporation of Cr in the Co_3O_4 lattice up to 33%. The Gaussian shape of the peaks up to 15% Cr substitution indicate pure cubic nature of the lattice; at higher Cr concentrations a doublet feature for all peaks

suggests coexistence of cubic and tetragonally distorted phases. Similar distortion was observed in a cubic fluorite structure of $CeZrO_2$ [36]. The doublet nature tends to become single peak again at 33% Cr doping as indicated by the lowest intensity of right side shoulder of the doublet. Moreover, the evolution of predominant lower angle peak with decreasing right shoulder peak indicates formation of more homogeneous tetragonally distorted phase. The crystallite size of the Cr/Co_3O_4 samples as calculated by above-mentioned procedure are presented in Table 1. It shows a systematic decrease of particle size, changing from 33 nm in Co_3O_4 to 18 nm in 14% Cr/Co_3O_4. Gradually decreasing crystallite size correlated in an increase in the surface area of the samples.

3.4 XAS studies

As XRD indicated substitution of Fe and Cr in the Co_3O_4 lattice, the site preference as well as homogeneity of substitutions were further analysed by X-ray Absorption Spectroscopic technique. Figure 5(a & b) show the X-ray absorption near edge structure (XANES) spectra of Cr and Fe in the doped Co_3O_4 samples measured at Cr and Fe K-edges, respectively. The shapes of the XANES spectra for all Cr containing Co_3O_4 are very similar indicating similar local coordination. The spectra demonstrate three main features: a small pre-edge peak (A) at about 5993.0 eV, a shoulder (B) at 6004.0 eV and an intensive white-line peak (C) at 6010.0 eV. Comparison to the literature data [37] suggests that chromium mainly present in a 3+ state and occupies a regular octahedral position in spinel structure similar to that in $FeCr_2O_4$. According to Fe K-edge XANES coordination of Fe in all Fe-doped Co_3O_4 samples is also octahedral and oxidation state is also close to 3+. All spectra demonstrate a small pre-edge at 7114.4 eV (A), a shoulder at 7128.4 eV (B) and an intense white-line peak at 7134.0 eV (C). Comparison of these

spectral features to literature [38] indicates that local symmetry and the oxidation state of Fe in Fe-Co_3O_4 samples is closer to those in α-Fe_2O_3 and goethite (FeOOH).

The EXAFS analysis for both Cr and Fe doped samples was performed on a Co_3O_4 cluster where central cobalt atom in octahedral position was substituted either by Fe or by Cr (Figure 6a & b). EXAFS spectra of all Cr and Fe doped Co_3O_4 samples were very similar, the octahedral coordination was matching well the experimental data and a high fit quality up to the 4^{th} coordination shell (Table 2). Preferential occupation of octahedral sites suggests very homogeneous distribution of dopant. Increase in Cr and Fe concentrations results in slightly increased local disorder indicated by the Debye-Waller factors (σ^2).

3.5 TEM studies

It is known that the catalytic activity of Co_3O_4 catalysts can vary depending on the nature of exposed crystallite surface, which determines the concentration of active sites including Co^{3+} atoms and low coordinated oxygen species. Therefore, surface morphologies of the crystallites have been carefully analyzed by TEM. Figure 7(a-f) presents the TEM images of as-prepared 15% Fe/Co_3O_4 (a,b), calcined 15% Fe/Co_3O_4 at 500 ^oC (c,d) and as-prepared 7% Cr/Co_3O_4 (e,f) samples. The low magnification images (7a, c) indicate minor growth of crystallites in calcined 15% Fe/Co_3O_4 in comparison with as-prepared sample. Similarly to as-prepared sample, calcined 15% Fe/Co_3O_4 (7b, d, respectively) sample expose mainly (111) and (220) planes. The (111) plane is predominant surface in both catalysts and in calcined catalyst and it has 20% higher population as calculated by distribution in several images. This proves that stability of surface morphology in Fe doped Co_3O_4 is significantly improved as (111) is the most stable and dominant surface. This can be correlated with stable catalytic activities. As catalytic activity in

as-prepared and calcined 15% Fe/Co_3O_4 samples are quite similar (showing 100% CO conversion below – 60 ^oC), the stability of (111) surface can explain the retaining of high activity.

A theoretical calculation has found that activation energies for CO oxidation on various crystal planes decrease in the order: (110) > (100) > (111) correlating to the concentration of Co^{3+} ions and low-coordinated oxygen species [25]. However, in the present study, (111) surface in Fe doped Co_3O_4 catalyst shows high catalytic activity similar to other catalysts prepared by other ambient synthesis method containing more active (100) or (110) surfaces [18,19]. Similarly, the analysis of 7%Cr/Co_3O_4 (Fig 7e, f) crystallites shows (220) and (111) as major crystal planes.

3.6 XPS studies

Detailed XPS studies of Fe and Cr doped Co_3O_4 catalysts can provide very useful information on the elemental oxidation states of the catalysts. XPS of Fe2p core level region in Fe doped Co_3O_4 catalysts with different Fe concentrations are presented in Fig. 8. Fe2p core level spectra are found to be broad which indicates that Fe is in multiple oxidation states. All the Fe2p core level spectra are curve-fitted into several component peaks. In Fig. 9, a typical curve-fitted $Fe2p_{3/2}$ spectrum of 20% Fe/Co_3O_4 catalyst is displayed. $Fe2p_{3/2}$ peaks observed at 709.8 and 711.3 eV correspond to Fe^{2+} and Fe^{3+} species, respectively present in the Fe/Co_3O_4 catalyst [39]. Fe^{2+} and Fe^{3+} species in Fe2p core level spectra are distinguished by their respective satellite peak positions. For Fe^{2+} species, intense satellite peak is situated around 4.5–5.5 eV above the main peak and a weak satellite peak related to Fe^{3+} species is observed around 7–9 eV above the main peak. In Figure 9, presence of both satellite peaks confirms that Fe^{2+} and Fe^{3+} are

present in the catalyst. It has been evaluated from XPS that Fe/Co_3O_4 catalysts contain mainly Fe^{3+} species along with certain amount of Fe^{2+} species. Surface concentrations of Fe^{2+} species vary from 24 to 26% in all the catalysts. This results correlate well with Fe Kedge XANES data demonstrating mainly presence of Fe^{3+} in all doped samples. Co2p core level spectra of these catalysts show that Co is present in both Co^{2+} and Co^{3+} states. The relative concentrations of Co^{3+} in the Fe/Co_3O_4 catalysts are found to be similar for all compositions (57 to 62%) as presented in Table 1. Similar ratios of Co^{3+}/Co^{2+} in the Fe doped Co_3O_4 samples explain high catalytic activity.

XPS of Cr2p core level region in Cr doped Co_3O_4 catalysts with different Cr concentrations are presented in Fig. 10. Observed $Cr2p_{3/2,1/2}$ peaks around 576.4 and 585.9 eV with 9.5 eV spin-orbit separation correspond to Cr^{3+} species [40]. Spectral envelopes of Co2p core level spectra are broad indicating that Co is present in different oxidation states. All the Co2p spectra are curve-fitted into sets of spin-orbit doublets along with associated satellite peaks. Accordingly, $Co2p_{3/2,1/2}$ peaks at 779.6 and 794.4 eV with spin-orbit separation of 14.8 eV correspond to Co^{3+}, whereas peaks at 781.3 and 796.8 eV with 15.5 eV spin-orbit separation are attributed to Co^{2+} species [41–43]. Binding energy peaks related to oxidized $Co2p_{3/2,1/2}$ species are located at 780.5 ± 1.5 and 796.0 ± 1.5 eV, respectively. Previous studies have reported that differences in the 2p peak positions between Co^{2+} and Co^{3+} vary from 0.1 to 1.5 eV making it difficult to use the primary 2p peaks for distinguishing between Co^{2+} and Co^{3+}. Similar to Fe2p core level spectra these two oxides can be distinguished, however, by the differences in the satellite features. The 2p spectrum of Co^{2+} contains prominent satellite peaks 4–6 eV higher in energy than the primary peaks.. On the other hand, Co^{3+} species is recognized by the presence of a weak satellite peak at 9–10 eV higher binding energy than the main peak. In the Cr/Co_3O_4

catalysts, the $Co2p_{3/2}$ peak around 781.3 eV along with the satellite peak at 784.4 eV are attributed to Co^{2+} species, whereas the $2p_{3/2}$ peak around 779.6 eV with the satellite peak at 789.7 eV are ascribed for Co^{3+} species. These satellite features arise from shake-up phenomenon in which the excitation of unpaired valence electrons increases the number of relaxed final states. It has been observed that Co^{2+} concentration increases with the increase in Cr concentration in Co_3O_4 matrix. This is because of the substitution of Cr^{3+} species into Co^{3+} sites of the Co_3O_4 substrate. Changes in Co^{2+} and Co^{3+} concentrations in Cr/Co_3O_4 catalysts evaluated from XPS analysis are summarized in Table 1. Typical curve-fitted Co2p spectra of 5% Cr/Co_3O_4 and 33% Cr/Co_3O_4 catalysts are given in Fig. 11.

3.7 H_2 TPR studies

The reducibility of Fe and Cr doped Co_3O_4 catalysts determine the catalytic property of these materials. Figure 12(a,b) presents the H_2 TPR profiles of the Fe and Cr doped Co_3O_4 samples with reference to the pure Co_3O_4. The reduction may occur in two consecutive steps: Co^{3+} (Co_3O_4) $\rightarrow$ Co^{2+} (CoO) and CoO $\rightarrow$ Co (metal). However, since redox reaction involving $Co^{3+} \leftrightarrow Co^{2+}$ couple on the surface determines the catalytic activity, hydrogen uptake corresponding to the lowest temperature region below 200 ^oC is discussed here. The huge signal above 250 ^oC is related to bulk reduction and hardly has effect on catalytic activity. As can be seen in the figure the reduction starts at 90 °C in pure Co_3O_4 and it gets shifted to 140 °C in all the Fe doped analogs up to 25% substitution, indicating similar nature of the reducing species. Previous study has shown that Fe^{3+} species in Fe_3O_4 gets reduced only above 200 °C despite of having similar structure to Co_3O_4 and the reduction is not related to low coordinated surface species. This confirms that low temperature peak occurs due to the reduction of Co^{3+} species and

at higher Fe doping the extent of reduction (area under the curve) may arise because of the interplay between the decreasing concentration of Co^{3+} and the increasing surface area of the material. The preferential reduction of Co^{3+} in comparison to Fe^{3+} species can probably be related to higher redox potential of the former ion. On the other hand, the low temperature reduction peak is consistently shifted with increasing Cr concentration from 105 ^{o}C in pure Co_3O_4 to 215 °C in 25% Cr doped samples. As we know that Cr^{3+} reduction is difficult and it is also difficult to get oxidized Cr^{4+} at such a low temperature, the presence of irreducible Cr^{3+} reduces the surface concentration of Co^{3+} and makes Co^{3+} less reducible, leading to lower activity of Cr doped catalysts. However, gradual increase in the extent of reduction is observed in these compounds, which correlates with the increase of the surface area. *Although, reduction with H_2 occurs at higher temperatures as compared to CO oxidation, the trend in reducibility of surface species can be correlated to the trend in the CO oxidation.*

3.8 CO_2 TPD studies

The basic character of the catalyst surface generally affects the catalytic activities due to formation of carbonate species preventing CO adsorption. Figure 13(a,b) shows temperature programmed desorption (TPD) profiles using acidic CO_2 as adsorbent for Fe and Cr doped Co_3O_4 samples. The intensity of corresponding CO_2 desorption peak indicates that larger amount of CO_2 has been adsorbed on Fe doped Co_3O_4 as compared to the Cr doped analogs. Interestingly, while concentration of desorbed CO_2 decreases with increasing Cr concentration, the opposite trend is observed with the Fe substitutions. Moreover, CO_2 desorption maxima in the Fe doped samples occur at higher temperature above ~100 ^{o}C as compared to Cr doped samples having CO_2 desorption peak at 65 ^{o}C. This means Fe doped Co_3O_4 samples form more stable carbonate species as compared with Cr doped analogs. Moreover, the observations clearly

indicate that Fe center creates basic sites and gets easily blocked with adsorbed CO_2. The increasing CO oxidation activity with Fe concentrations in Fe/Co_3O_4 samples despite increasing CO_2 coverage indicate that Fe site do not take part in CO adsorption leading to oxidation. On the other hand, decrease in CO oxidation activity with increasing Cr doping also indicates that Cr is not involved in CO adsorption as well as CO oxidation. Further, CO_2 desorption decreases with decreasing Co^{3+} concentrations in Cr doped catalysts (see XPS section, Table 1). Therefore, it can be concluded that Co^{3+} acts as active site for CO adsorption as well as CO oxidation reaction in presence of both type of dopant cations.

4. Conclusions

Fe and Cr substituted Co_3O_4 oxides prepared by single step solution combustion method result in homogeneous solid solutions with spinel structure. Both Fe and Cr substitute cobalt in the octahedral sites of the Co_3O_4 structure. The oxidation state of Fe remains mainly +3 and Cr is present exclusively in +3 oxidation state. While relative concentration of Co^{3+} on the surface remains almost identical in all Fe doped Co_3O_4 catalysts, the same decreases for non-redox Cr doped Co_3O_4 catalysts. The main crystal planes detected in Fe and Cr doped catalysts are (111) and (220). While Fe/Co_3O_4 compositions have achieved maximal activity on 15% Fe/Co_3O_4 with T_{50} at −85 °C and preserved it almost unchanged up to 25% Fe substitution, the incorporation of Cr^{3+} decreased the activity up to 33% substitutions passing through a maximum activity for 7% Cr with T_{50} at −42 °C. The (111) plane is the most stable surface in 15% Fe/Co_3O_4 and its presence increases after calcinations. The CO oxidation activities correlate with the concentration of Co^{3+} ion present on the surface creating redox site for low temperature reaction. The lowest temperature H_2 consumption peak related to the surface reduction in H_2-TPR gets

maximal intensity at 15% Fe substitution and does not change at higher Fe concentrations, which indicate that similar amount of Co^{3+} ions is present on the surface of all Fe doped samples, assuming that Fe^{3+} reduction occurs above 200 °C. Therefore, CO conversion reaches maximum at 15% Fe substitution and after remains unchanged. At the same time, for Cr doped samples the activity reaches the highest value for 7% Cr substitution showing 100% conversion at −32 °C and then consistently decreases. This happens because Co^{3+} concentration decreases with Cr^{3+} substitution. The initial increase in activity with low Cr doping can be due to higher surface area and lowering of activity at higher concentrations is due to stronger Cr–O bond.

Acknowledgement

We thank Dr. Frank Krumeich for the electron microscopy study, which was performed at EMEZ (Electron Microscopy ETH Zurich).

References

1. A.V. Nero Jr., Sci. Am. 258 (1998) 24.
2. M. Jacoby, Chem. Eng. News 2003, January 20, p. 32.
3. R. Jain, US Patent 5 110 569, 1992.
4. N. Funasaki, A. Henmi, S. Ito, Y. Asano, S. Yamashita, T. Kobayashi, M. Haruta, Sensor. Actuat. B 14 (1993) 536.
5. M. Haruta, N. Yamada, T. Kobayashi and S. Iijima, J. Catal., 1989, 115, 301.
6. M. Haruta, T. Kobayashi, H. Sano and N. Yamada, Chem. Lett., 1987, 16, 405.
7. M. Haruta, J. New Mater. Electrochem. Sys. 7 (2004) 163-172
8. F.S. Stone, Adv. Catal. 13 (1962) 1.

9. M. Haruta, M. Yoshizaki, D.A.H. Cunningham, T. Iwasaki, Ultra Clean Technol. 8 (1996) 117 (in Japanese).
10. Y. Teng, H. Sakurai, A. Ueda, T. Kobayashi, International Journal of Hydrogen Energy 13, 1999, 244-247.
11. Jonas Jansson, Journal of Catalysis **194,** 55–60 (2000)
12. Jonas Jansson, Anders E. C. Palmqvist, Erik Fridell, Magnus Skoglundh, Lars Osterlund, Peter Thormahlen, Vratislav Langer, Journal of Catalysis **211,** 387–397 (2002)
13. E.C. Njagi, C.-H. Chen, H. Genuino, H. Galindo, H. Huang, S.L. Suib, Appl. Catal.B: Environ. 99 (2010) 103–110.
14. F. Grillo, M.M. Natile, A. Glisenti, Appl. Catal. B: Environ. 48 (2004) 267–274.
15. C. Xu, Y. Liu, C. Zhou, L. Wang, H. Geng, Y. Ding, ChemCatChem 3 (2011) 399–407.
16. H. Tüysüz, M. Comotti, F. Schüth, Chem. Commun. (2008) 4022–4024.
17. D. A. H. Cunningham, T. Kobayashi, N. Kamijo, M. Haruta, Catal. Lett. 25 (1994) 257-264.
18. X. Xie, L. Li, Z.-Q. Liu, M. Haruta, W. Shen, Nature 458 (2009) 746–749.
19. Y. Yu, T. Takei, H. Ohashi, H. He, X. Zhang, M. Haruta, J. Catal. 267 (2009) 121–128.
20. Ying jun Fenga, Liang Li, Shufan Niua, Yan Qua, Qian Zhang, Yongsheng Li,Wenru Zhao, Hua Li, Jianlin Shi, Applied Catalysis B: Environmental 111– 112 (2012) 461–466.
21. Arti Dangwal Pandey, Chunjiang Jia, Wolfgang Schmidt, Matteo Leoni, Manfred Schwickardi, Ferdi Schüth, and Claudia Weidenthaler, J. Phys. Chem. C 2012, 116, 19405−19412.
22. A.T. Bell, Science 299 (2003) 1688.

23. Yonghong Teng, Yoshihiro Kusano, Masaki Azuma, Masatake Haruta, Yuichi Shimakawa, Catal. Sci. Technol., 2011, **1**, 920–922.
24. De-en Jiang, Sheng Dai, *Phys. Chem. Chem. Phys.*, 2011, **13**, 978–984
25. Hai-Feng Wang, Richard Kavanagh, Yang-Long Guo, Yun Guo, Guanzhong Lu, P. Hu, Journal of Catalysis 296 (2012) 110–119.
26. Yang-Gang Wang, Xiao-Feng Yang, Jun Li, Chinese Journal of Catalysis 37 (2016) 193–198.
27. Jie Li, Guanzhong Lu, Guisheng Wu, Dongsen Mao, Yanglong Guo, Yanqin Wang, Yun Guo, RSC Advances, 2013, 3, 12409.
28. Gengnan Li, Liang Li, Yongsheng Li, Jianlin Shi, New J. Chem., 2015, 39, 1742
29. Kohji Omata, Takashi Takada, Seiji Kasahara, Muneyoshi Yamada, Applied Catalysis A: General 146 (1996) 255-267.
30. Yang Lou, Jian Ma, Xiaoming Cao, Li Wang, Qiguang Dai, Zhenyang Zhao, Yafeng Cai, Wangcheng Zhan, Yanglong Guo, P. Hu, Guanzhong Lu, Yun Guo, ACS Catal. 2014, 4, 4143−4152.
31. Yang Lou, Li Wang, Zhenyang Zhao, Yanhui Zhang, Zhigang Zhang, Guanzhong Lu, Yun Guo, Yanglong Guo, Applied Catalysis B: Environmental 146 (2014) 43– 49.
32. Patil, K. C.; Aruna, S. T.; Mimani, T. *Curr*. *Opin*. *Solid State Mater*. *Sci*. **2002**, *6*, 507.
33. M. S. Hegde, K. C. Patil and G. Madras, Acc. Chem. Res., 2009, 42, 704.
34. ----XXXXX
35. Dong Gu, Chun-Jiang Jia, Claudia Weidenthaler, Hans-Josef Bongard, Bernd Spliethoff, Wolfgang Schmidt, Ferdi Schüth, J. Am. Chem. Soc. 2015, 137, 11407−11418.

36. Masatomo Yashima,* Kenji Morimoto, Nobuo Ishizawa, and Masahiro Yoshimura, J. Am. Ceram. Soc. **1993**, 76, 2865-68.

37. F. Farges, Phys. Rev. B: Condens. Matter Mater. Phys., 2005, 71, 155109.

38. M. Wilke, F. Farges, P.-E. Petit, G. E. Brown Jr., F. Martin, 2001, 86, 714.

39. J. F. Moulder, W. F. Stickle, P. E. Sobol and K. D. Bomben, Handbook of X-ray Photoelectron Spectroscopy, Ed. J. Chastain, Perkin-Elmer Corporation, Eden Prairie, 1992.

40. C. Anandan, V. K. W. Grips, K. S. Rajam, V. Jayaram and P. Bera, Appl. Surf. Sci., 2002, 191, 254.

41. L. Li, T. Sasaki, Y. Shimizu and N. Koshizaki, J. Phys. Chem. C, 2009, 113, 15948.

42. S. C. Petitto and M. A. Langell, J. Vac. Sci. Technol. A, 2004, 22, 1690.

43. P. Bera, H. Seenivasan, K. S. Rajam, C. Shivakumara and S. K. Parida, Surf. Interface Anal. 2013, 45, 1026.

Table 1. Crystalilite size calculated using Scherrer formula, BET surface area and surface Co^{3+} concentration in the Fe/Co_3O_4 and Cr/Co_3O_4 samples

Catalysts	**Crystallite size (nm) (using Scherrer formula)**	**BET surface area (m^2g^{-1})**	**Co^{3+} concentration from XPS $[Co^{3+}/(Co^{3+} + Co^{2+})]$%**
	Fe/Co_3O_4		
Co_3O_4	33	12.73	66.66
3%Fe/Co_3O_4	28	XX	61
7%Fe/Co_3O_4	23	XX	62
10%Fe/Co_3O_4	22	-	64
15%Fe/Co_3O_4	17	XX	57
20%Fe/Co_3O_4	16	-	58
25%Fe/Co_3O_4	14	XX	62

		Cr/Co₃O₄	
1%Cr/Co_3O_4	36	12.73	-
3%Cr/Co_3O_4	28	25.26	61
5%Cr/Co_3O_4	28	26.39	60
7%Cr/Co_3O_4	23	28.56	58
10%Cr/Co_3O_4	22	42.79	57
15%Cr/Co_3O_4	18		55
20%Cr/Co_3O_4	-		-
25%Cr/Co_3O_4	-		-
33%Cr/Co_3O_4	-		51

Table 2. Local coordination of Cr and Fe in Co_3O_4 structure analyzed by Cr K-edge and Fe K-edge EXAFS

Sample	Neighbor	Number	σ^2, Å^2	R, Å	ΔE_0	S_0^2
Cr/Co_3O_4 samples						
3%Cr/Co_3O_4	O	6	0.0025(6)	1.97(1)	2.6(1.0)	0.66
	Co	6	0.0030(5)	2.90(1)		
	Co	6	0.0066(8)	3.39(1)		
	Co	12	0.0049(9)	5.00(2)		
7%Cr/Co_3O_4	O	6	0.0028(5)	1.97(1)	0.7(1.0)	0.66
	Co	6	0.0038(4)	2.90(1)		
	Co	6	0.007(1)	3.39(1)		
	Co	12	0.0059(9)	5.00(2)		
10%Cr/Co_3O_4	O	6	0.0028(5)	1.97(1)	0.48(1.0)	0.66
	Co	6	0.0035(3)	2.90(1)		
	Co	6	0.007(1)	3.39(1)		
	Co	12	0.006(1)	5.00(2)		
Fe/Co_3O_4 samples						
3%Fe/Co_3O_4	O	6	0.0057(7)	1.99(1)	1.0(1.3)	0.88
	Co	6	0.0063(5)	2.91(1)		
	Co	6	0.0081(8)	3.39(1)		
	Co	12	0.0070(8)	4.96(1)		
10%Fe/Co_3O_4	O	6	0.0061(1)	1.99(1)	0.7(1.2)	0.88
	Co	6	0.0071(5)	2.91(1)		
	Co	6	0.0089(9)	3.41(1)		
	Co	12	0.009(1)	4.97(2)		
15%Fe/Co_3O_4	O	6	0.0068(7)	1.99(1)	0.3(1.2)	0.88
	Co	6	0.0078(6)	2.92(1)		
	Co	6	0.0093(9)	3.41(1)		
	Co	12	0.010(1)	4.99(2)		
25%Fe/Co_3O_4	O	6	0.0080(7)	1.99(1)	1.3(1.2)	0.88
	Co	6	0.0094(6)	2.92(1)		
	Co	6	0.012(1)	3.41(1)		
	Co	12	0.012(1)	4.99(2)		

Figures

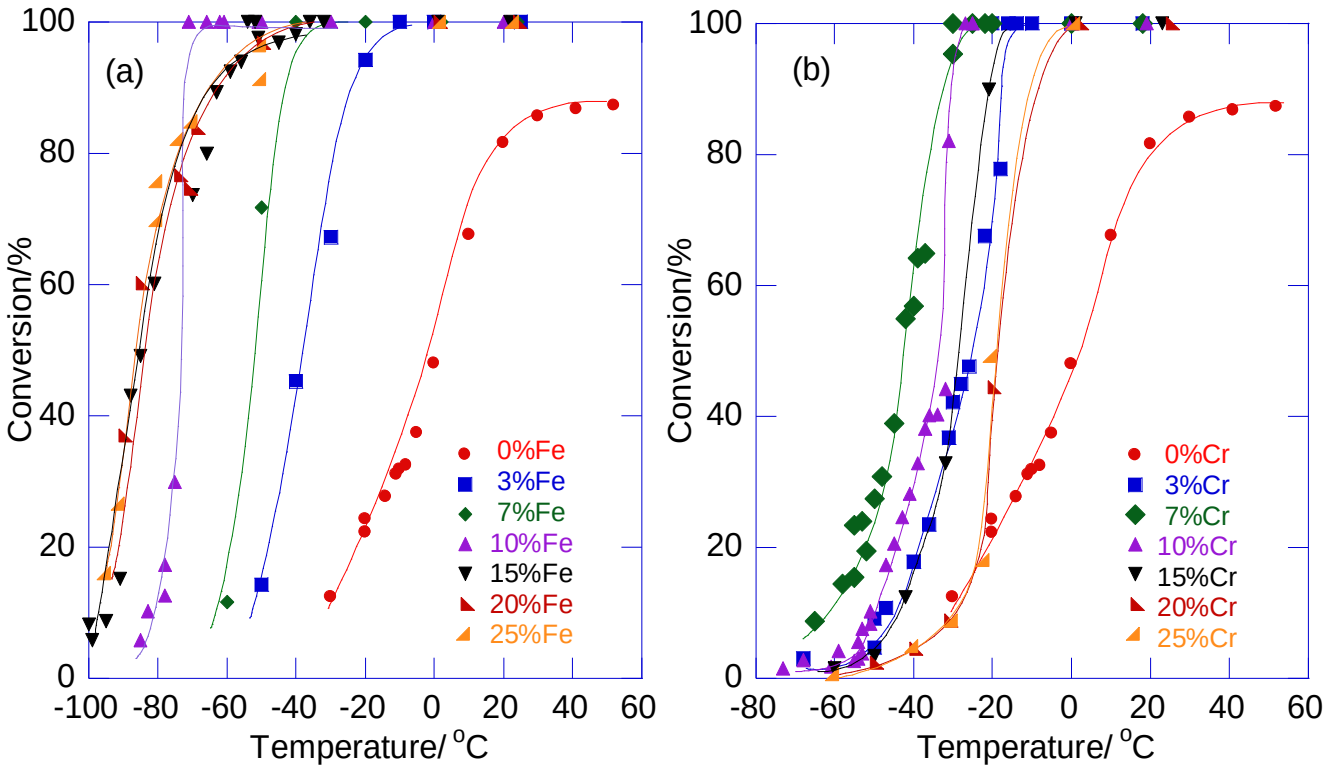

Figure 1. CO conversion as a function of Temperature over (a) Fe/Co_3O_4 and (b) Cr/Co_3O_4 samples

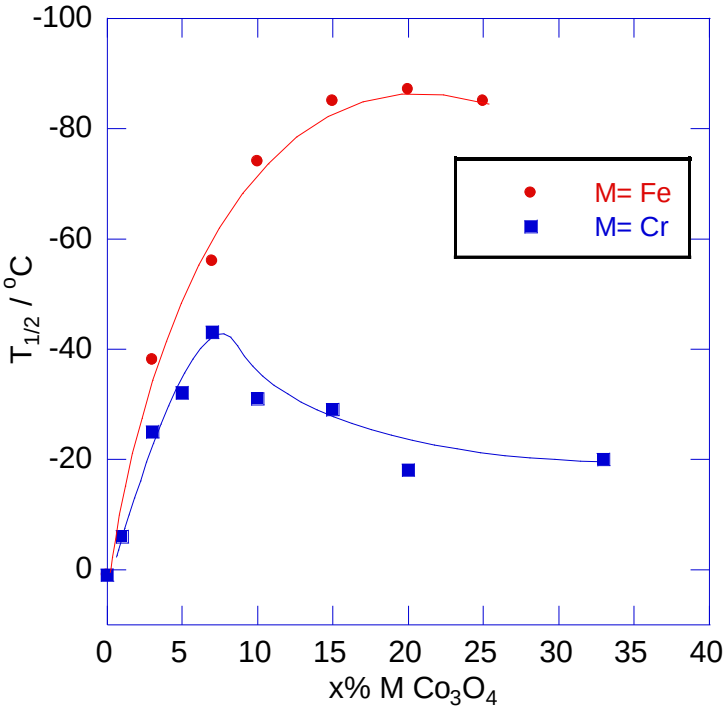

Figure 2: T_{50} for CO conversion vs Concentration of Fe and Cr dopants in Co_3O_4

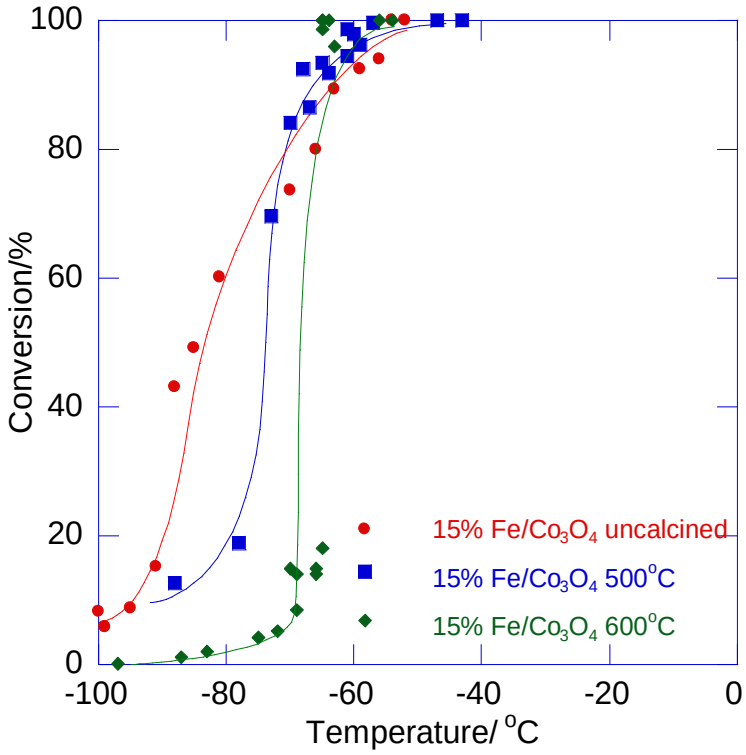

Figure 3: CO conversion as a function of Temperature over 15%Fe/Co_3O_4 calcined at different temperatures

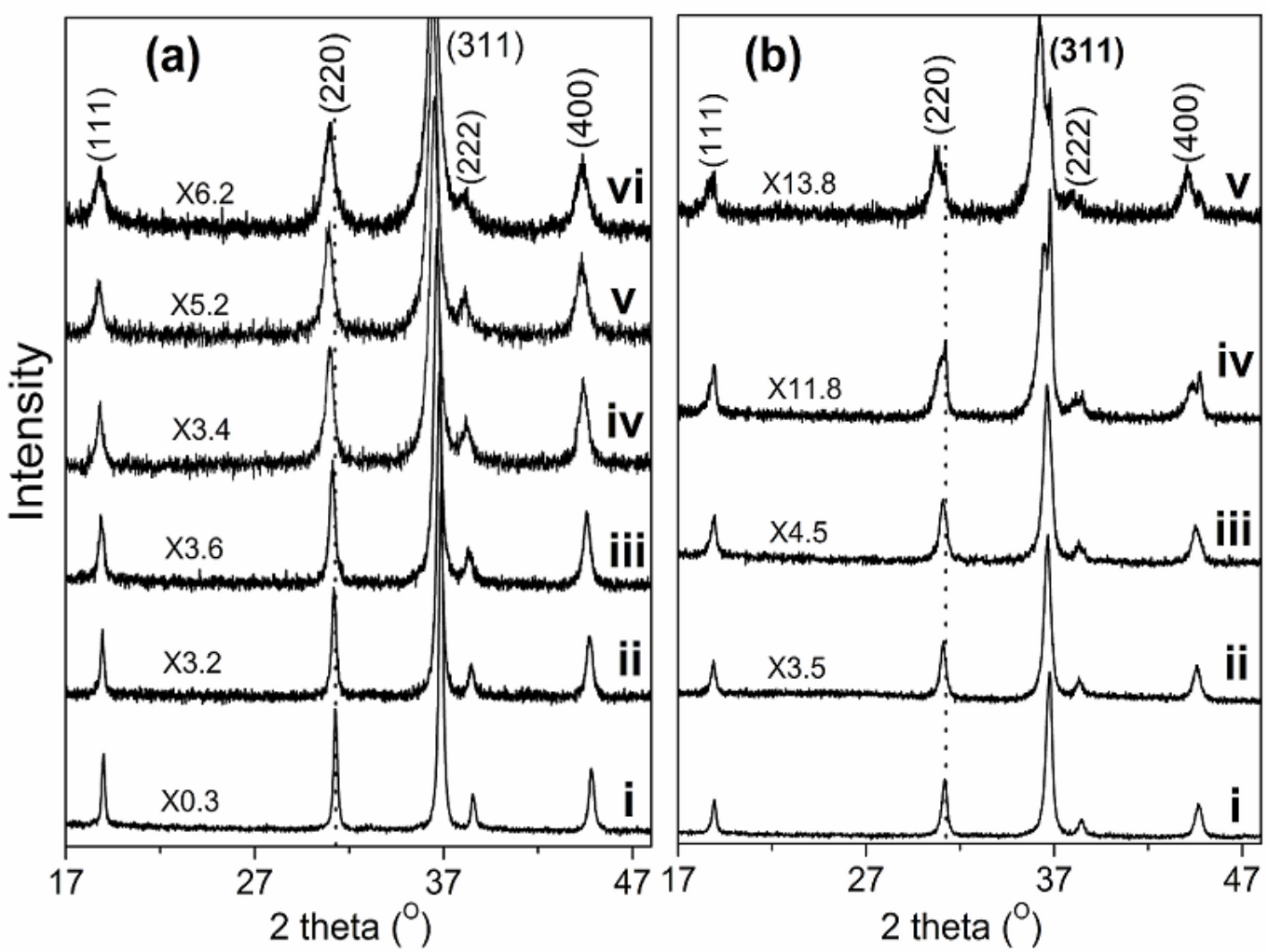
(a)
(111)
(220)
(311)
(222)
(400)
X6.2
vi
X5.2
v
X3.4
iv
X3.6
iii
X3.2
ii
X0.3
i
Intensity
17
27
37
47
2 theta (°)
(b)
(311)
(111)
(220)
(222)
(400)
X13.8
v
X11.8
iv
X4.5
iii
X3.5
ii
i
17
27
37
47
2 theta (°)

Figure 4. XRD profiles of (a) Fe/Co_3O_4 catalysts: (i) Co_3O_4, (ii) 3% Fe/Co_3O_4, (iii) 10% Fe/Co_3O_4 (iv) 15% Fe/Co_3O_4, (v) 20% Fe/Co_3O_4 and (vi) 25% Fe/Co_3O_4 ; (b) Cr/Co_3O_4 catalysts: (i) 7% Cr/Co_3O_4, (ii) 10% Cr/Co_3O_4, (iii) 15% Cr/Co_3O_4, (iv) 20% Cr/Co_3O_4 and (v) 33% Cr/Co_3O_4.

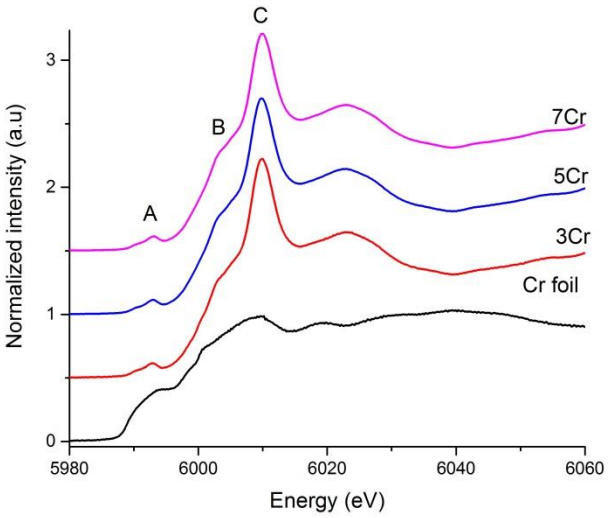

Fig. 5a. Cr K-edge XANES of Cr doped Co3O4 containing 3, 5 and 7% of Cr in comparison to the Cr foil

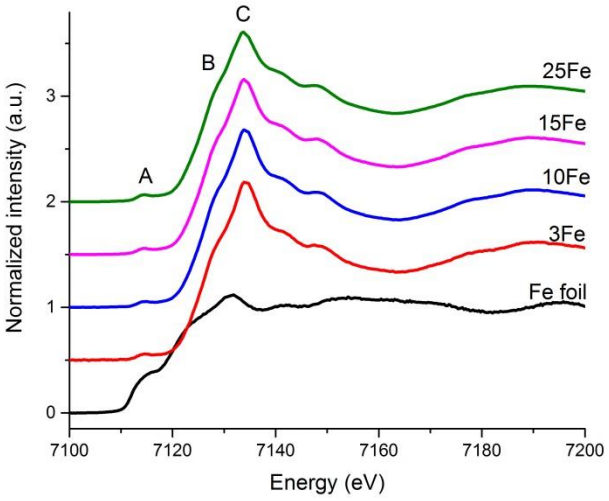

Fig.5b. Fe K-edge XANES of Fe doped Co3O4 containing 3, 10, 15 and 25% of Fe in comparison to the Fe foil.

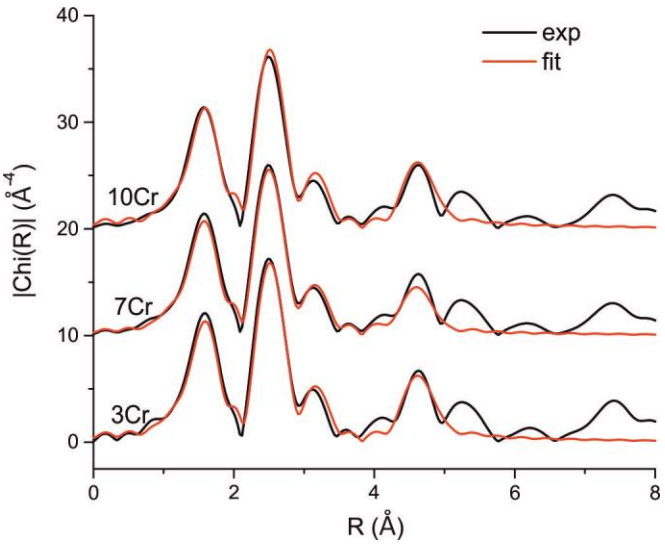

Fig. 6a. Fit of the Cr K-edge EXAFS spectra between 1 and 5 Å for Cr doped Co3O4 containing 3, 5 and 7 % of Cr

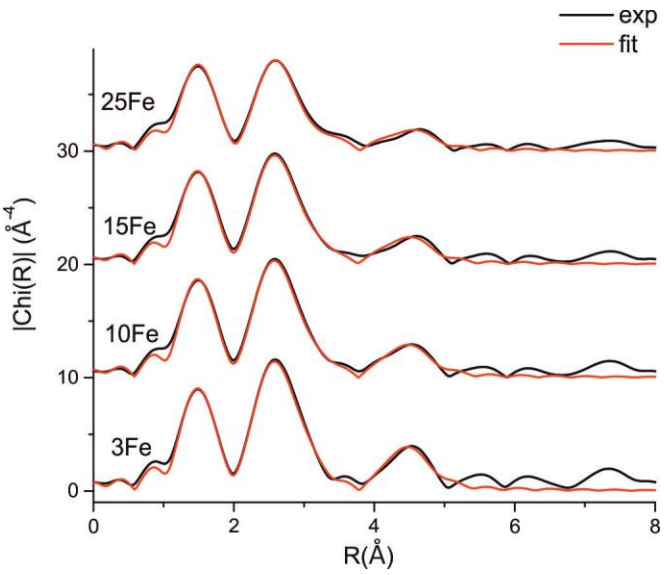

Fig. 6b. Fit of the Fe K-edge EXAFS spectra between 1 and 5 Å for Fe doped Co_3O_4 containing 3, 10, 15 and 25% of Fe

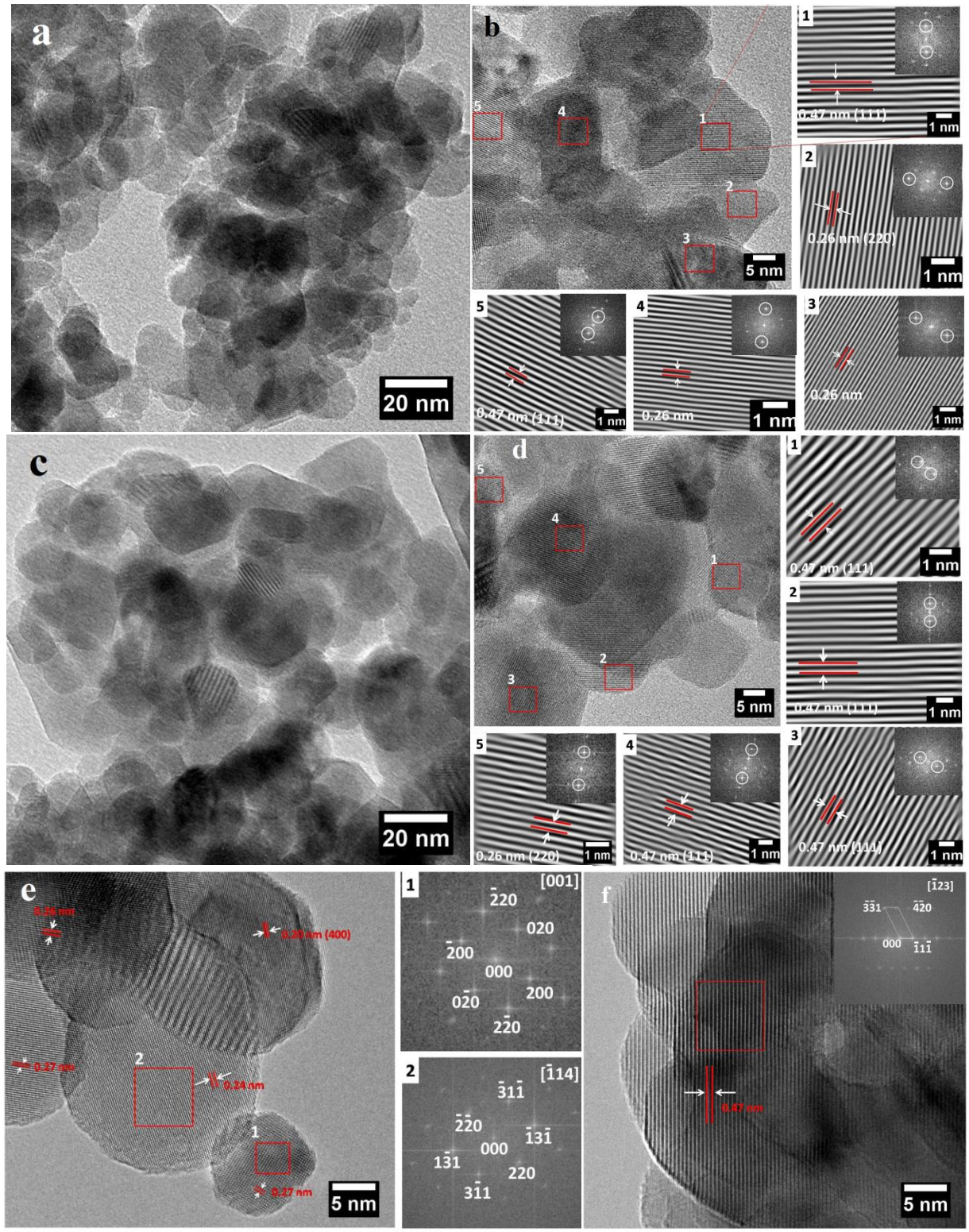

Figure 7. TEM images of as-prepared 15%Fe/Co_3O_4 (a,b), calcined 15%Fe/Co_3O_4 (c,d) and as-prepared 7%Cr/Co_3O_4 (e,f) catalysts

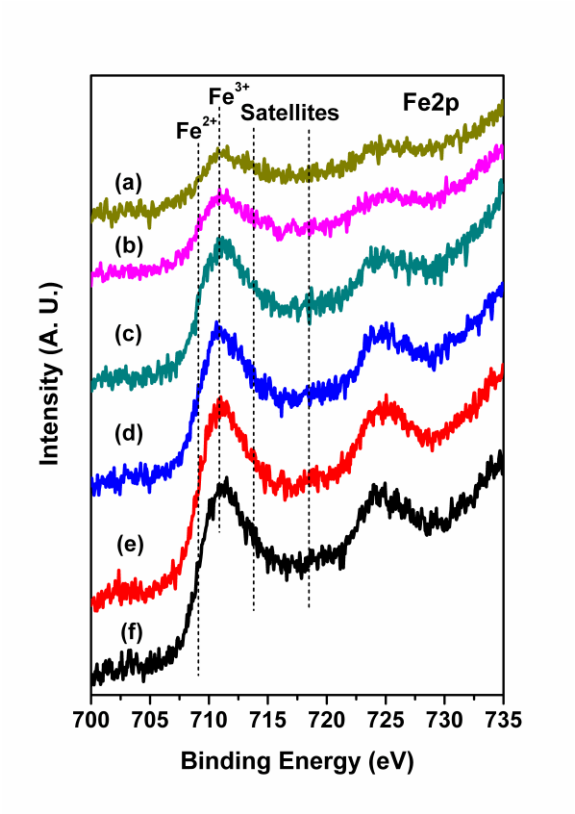

Fig. 8. XPS of Fe2p core levels in Fe/Co_3O_4 catalysts: (a) 3% Fe/Co_3O_4, (b) 7% Fe/Co_3O_4, (c) 10% Fe/Co_3O_4, (d) 15% Fe/Co_3O_4, (e) 20% Fe/Co_3O_4 and (f) 25% Fe/Co_3O_4.

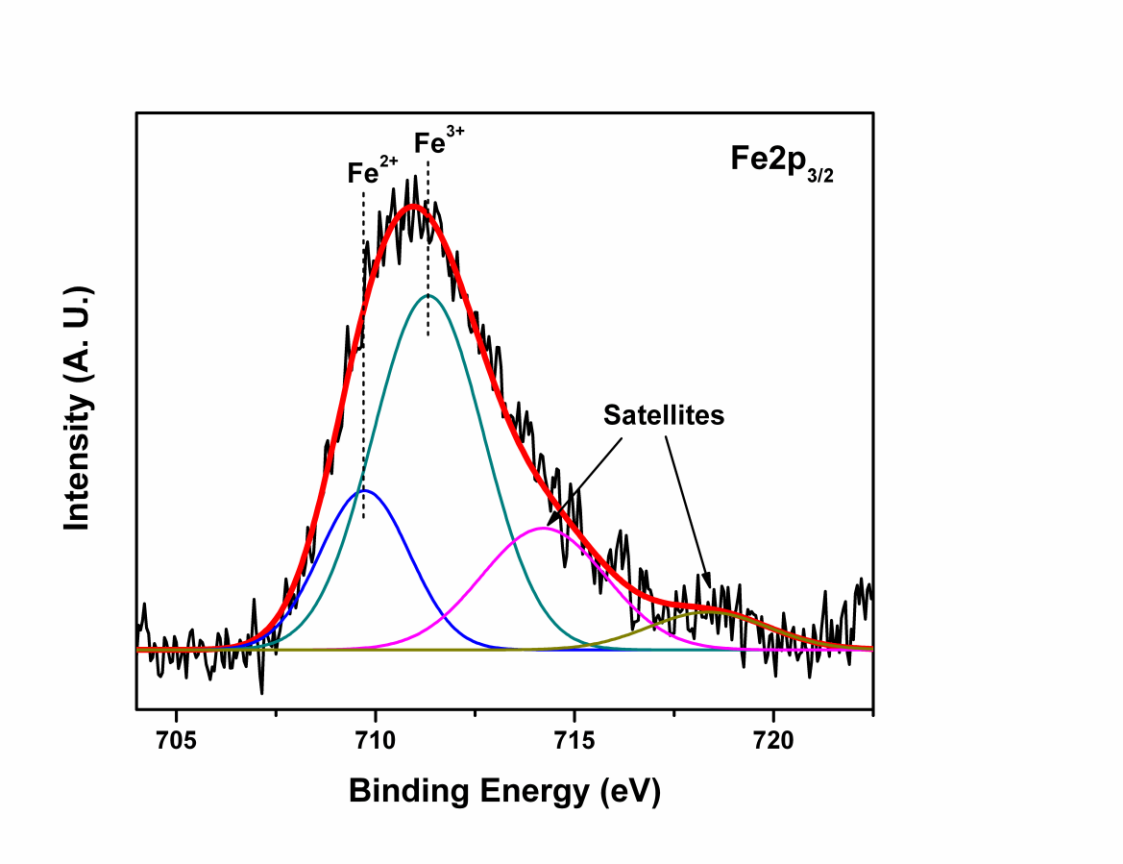

Fig. 9. Curve-fitted XPS of Fe2p core level in 20% Fe/Co_3O_4 catalyst.

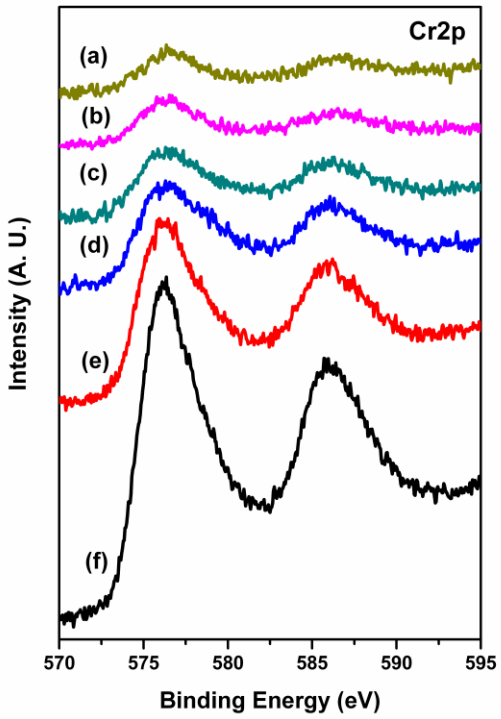

Fig. 10. XPS of Cr2p core levels of Cr/Co_3O_4 catalysts: (a) 3% Cr/Co_3O_4, (b) 5% Cr/Co_3O_4, (c) 7% Cr/Co_3O_4, (d) 10% Cr/Co_3O_4, (e) 15% Cr/Co_3O_4 and (f) 33% Cr/Co_3O_4.

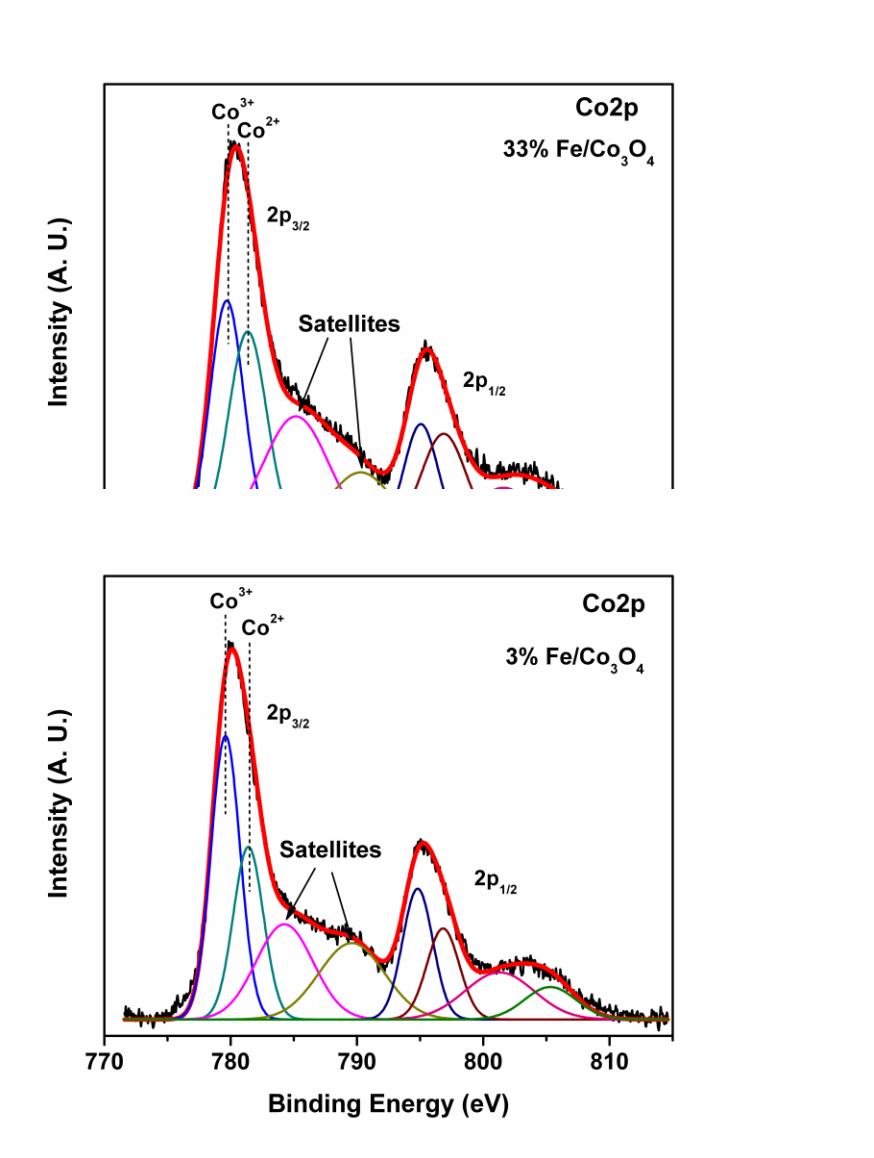

Fig. 11. Curve-fitted XPS of Co2p core levels of 3% Cr/Co_3O_4 and 33% Cr/Co_3O_4 catalysts.

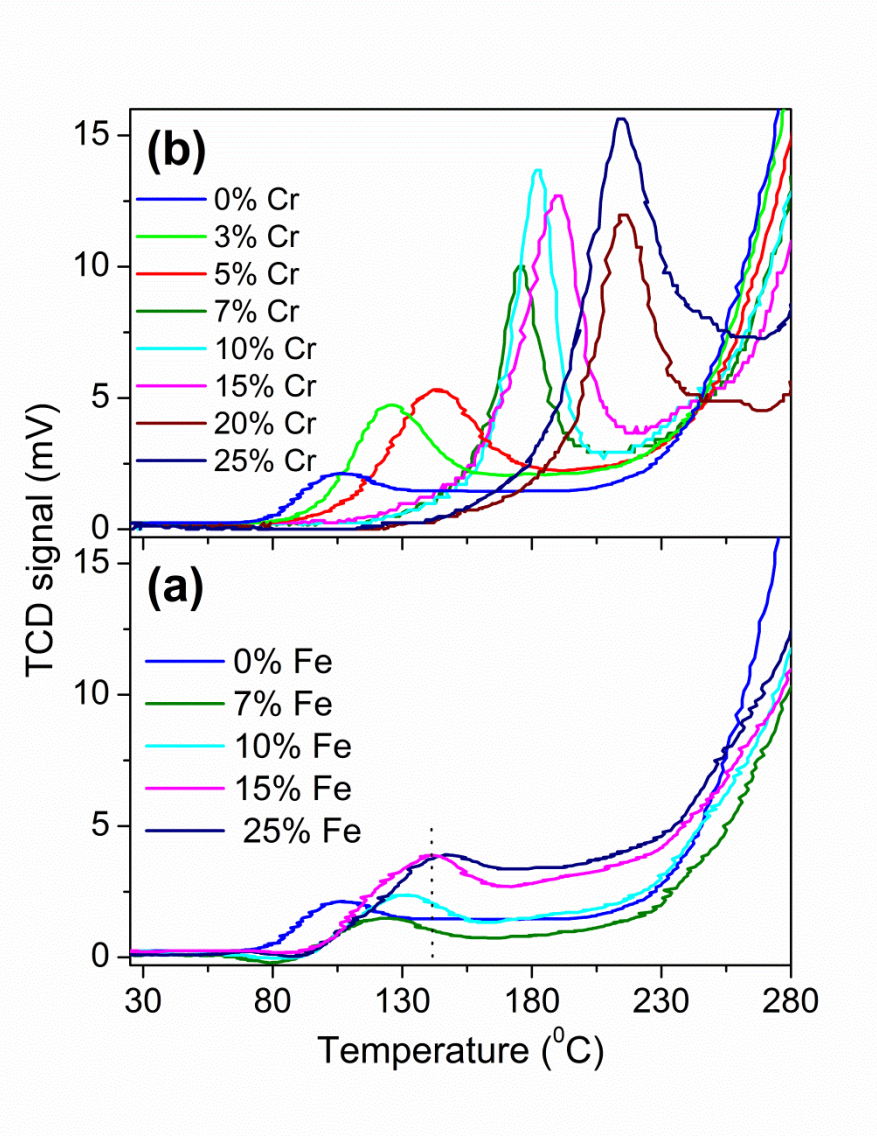

Figure 12. H_2 TPR profiles for Fe/Co_3O_4 (a) and Cr/Co_3O_4 (b) catalysts

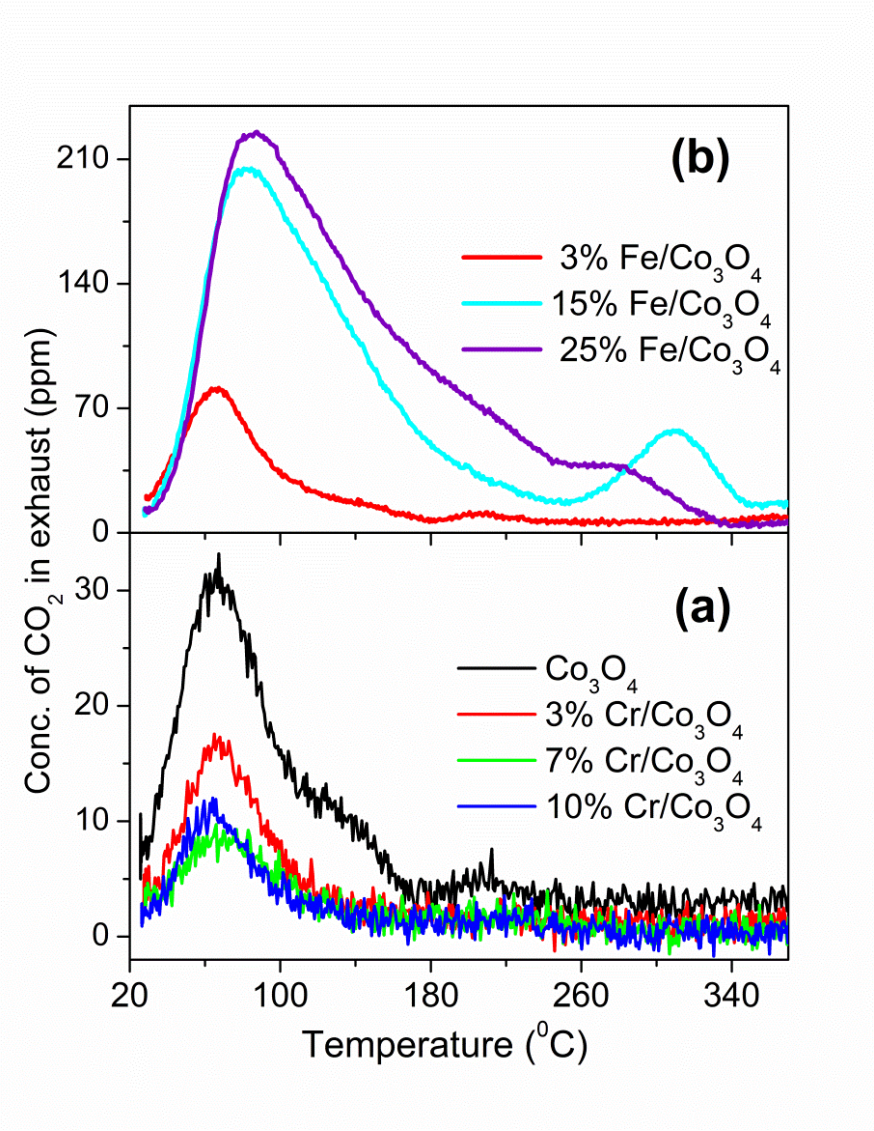

Figure 13. CO_2 TPD profiles for Cr/Co_3O_4 (a) and Fe/Co_3O_4 (b) catalysts

Supplementary Figures

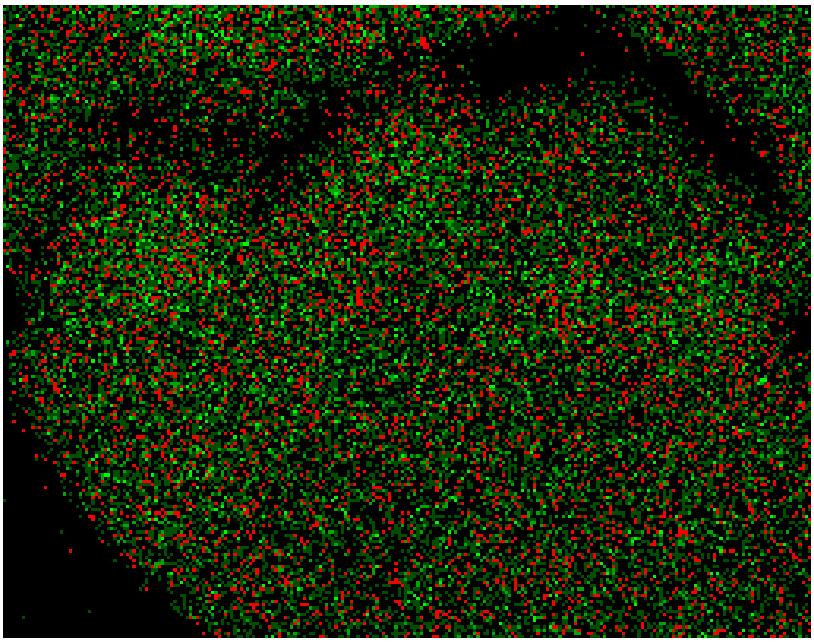

Figure S1. Elemental maps of Co (Green) and Fe (Red) obtained by TEM analysis

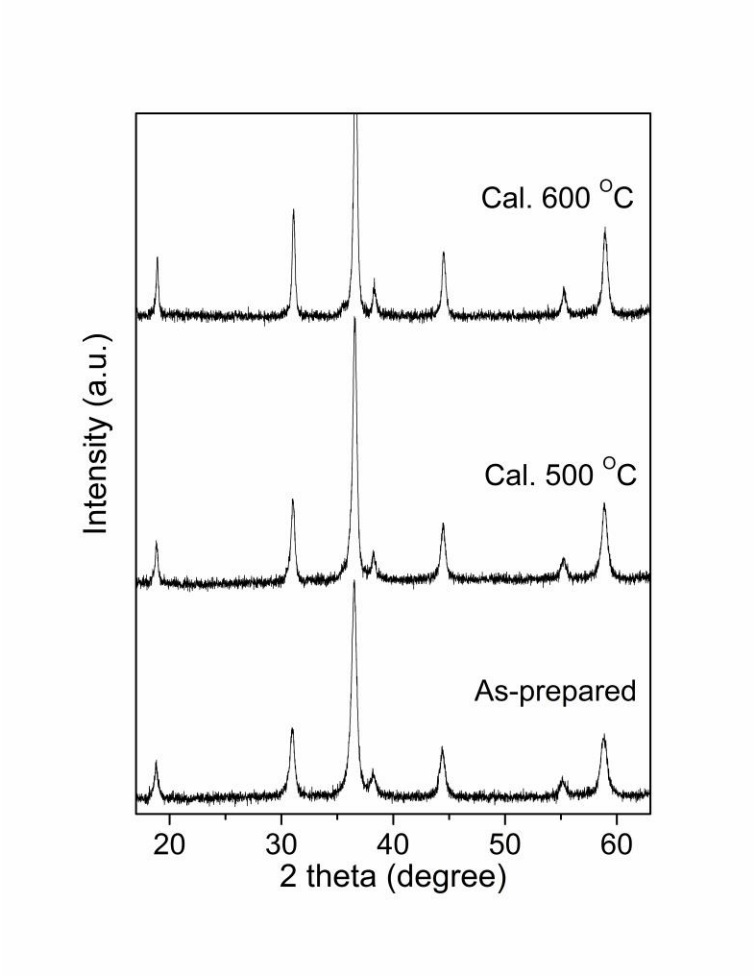

Figure S2. XRD profiles of as-prepared and calcined 15%Fe/Co_3O_4 samples.